Journal of Sound and Vibration (2002) **258**(5), 931–949
doi:10.1006/jsvi.2002.5135, available online at http://www.idealibrary.com on IDEAL®

A HYBRID FINITE SEGMENT/FINITE ELEMENT MODELLING AND EXPERIMENT ON A FLEXIBLE DEPLOYMENT SYSTEM

Y. Cheng, S. L. Dai and G. X. Ren

Department of Engineering Mechanics, Tsinghua University, Beijing 100084, *People's Republic of China. E-mail*: *ycheng99@mails.tsinghua.edu.cn*

(*Received* 26 *July* 2001, *and in final form* 21 *March* 2002)

This paper focuses on the dynamic responses of a flexible deployment system that has a central rigid body and four articulated flexible beams and undergoes locking impact. A hybrid finite segment/finite element model and an experiment are presented for the deployment system. The flexible beam components in the system are modelled with the finite segments connected by massless beam elements, wherein the finite segments describe the inertia of the large rotation flexible beam and the massless elastic elements describe the elasticity of the flexible beam by taking the advantage of small deformation in the relative co-ordinate system. To model the internal impacts in the articulate joints due to clearances, a continuous contact force model of locking joint is also proposed. The governing differential–algebraic equations of the system are established by the Newton–Euler method with Lagrange multipliers and are solved with the method of generalized co-ordinate partitioning. To accelerate the numerical integration, a "longitudinal constraint" is suggested to alleviate the stiff problem of the dynamic equations. In addition, a physical model of the deployment system is constructed. The deployment is released by the compressed springs in the joints. A position measuring system of linear CCD cameras is used to measure the large displacement of the system. Correlations between the mathematical model and the experiments are also presented. Reasonable results are obtained.

1. INTRODUCTION

The deployment system is generally characterized by the coupled rigid-body motion and the elastic vibration, and the dynamics of which is further complicated by the internal impacts in the connecting joints of the system. The modelling of such system involves two main aspects, namely the modelling of the elastic body with large displacement and that of the impacts in the joints.

The assumed mode method has dominated the history of dynamics of structures for a long time. It generally involves few degrees of freedom and gives clear physical explanation. So this method has been introduced to the fields of multi-body systems. However, it is devoid of the flexibility for describing complicated systems with complex boundary or time-varying boundary conditions. With the advent of modern computer technology and development of computational mechanics, the finite element method has been widely used in the fields of multi-body system [1–5]. On the other hand, Huston and Connelly [6–8] developed the finite segment approach for elastic slender beams in multi-body system, in which each beam is modelled as a collection of rigid segments connected

0022-460X/02/$35.00

by linear springs and dampers. In this method, the coupled problem of the rigid-body motion and flexible vibrations is transformed into that of a rigid-multi-body system. Based on finite segment approach, Zakhariev [9] suggested a method of finite elements in relative co-ordinates for the solution of non-linear elastic problems of large deformation. In the finite segment approach, the large deformation of the flexible structure could be represented by the small deformation in the relative co-ordinate system and rigid-body motion of the segment. As a result, the geometric non-linear and non-linear inertia effects are naturally taken into account.

The impact problems in multi-body systems have drawn the attentions of many researchers [10–17]. Khulief and Shabana [10–12] investigated the impact responses in a constrained mechanical system with flexible components through the momentum balance method, in which a set of impulse–momentum relations is solved to account for the jump discontinuities in velocity. Nagaraj *et al.* [13] applied the same method to a two-link flexible system undergoing locking. On the other hand, Dubowsky and Gardner [14] developed an "impact-beam" model, wherein the impact force was modelled by a force-displacement law with the material compliance. Hunt and Grossley [15] presented a contact force model by the Hertz force displacement law, and suggested a hysteresis damping. Lee and Wang [16] introduced a hysteresis damping function that characterizes the speed and load-dependent nature of damping. Yigit *et al.* [17] used the model developed by Lee and Wang for the dynamics of a radially rotating beam with impact and excellent agreement was found between the simulation and the experiments. Compared with the momentum balance method, the continuous contact force model can give information concerning the contact force. However, it requires additional parameters to be determined.

In this paper, the hybrid method of finite segment and beam element together with continuous contact force model of impact are used for dynamic modelling of a deployment system with a central rigid body and four articulated flexible beams. A brief description of the flexible deployment system is given in section 2 and the dynamic equations of flexible multi-body system with internal impact are established in section 3. A "longitudinal constraint" is suggested to decrease the stiffness of the equations in section 4. The simulation results of the deployment system are presented in section 5. Finally, the experimental set-up and results are presented and are compared with numerical simulation.

2. DESCRIPTION OF THE FLEXIBLE DEPLOYMENT SYSTEM

The deployment system investigated in this paper is shown in Figure 1. It includes a central rigid body and four articulated flexible beams. The system is folded into an initial position, as shown in Figure 1(a), and is expanded by releasing the compressed torsion springs in the joints. In the deployment, the beams experience both large rigid-body motions and elastic vibrations, as shown in Figure 1(a)–1(d). When joints are locked at appropriate positions, the impacts in the joints will induce elastic vibrations.

3. DYNAMIC MODELLING OF THE FLEXIBLE DEPLOYMENT SYSTEM

The purpose of this section is to establish the dynamic equations of the deployment system described in the above section. Section 3.1 deals with the finite segment modelling of the flexible beams that experience large rigid-body motions. Section 3.2 introduces the

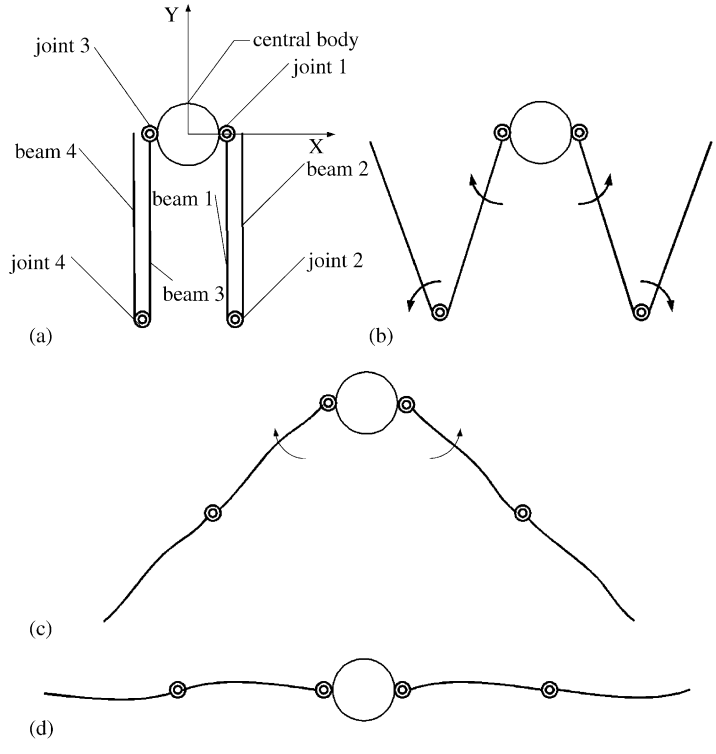

Figure 1. Schematic representation of motion of four-beam flexible system with a central rigid body: (a) initial configuration; (b) initial movement; (c) motion after first locking; (d) end configuration.

mathematical model of the locking impacts in the joints and section 3.3 establishes the dynamic equations of motion of the flexible deployment system.

3.1. MODELLING OF THE FLEXIBLE BEAMS

The modelling of the flexible beams includes two parts, namely the inertial modelling with the finite segment and the elastic modelling with the finite element.

3.1.1. *The inertia modelling*

In the finite segment approach, the flexible beam is discretized into a number of rigid segments connected by beam elements, as shown in Figure 2.

The virtual work equation for the discrete flexible beam s can be expressed as

$$\delta \mathbf{q}_s^{\mathrm{T}} [\mathbf{M}_s \ddot{\mathbf{q}}_s - \mathbf{Q}_s] = 0, \tag{1}$$

where $\mathbf{M}_s$ is the mass matrix, $\mathbf{q}_s$ is the generalized co-ordinate vector and $\mathbf{Q}_s$ is the corresponding generalized force vector, which are defined as follows:

$$\mathbf{q}_s = \left[\mathbf{q}_{s1}^{\mathrm{T}}, \mathbf{q}_{s2}^{\mathbf{T}}, \ldots, \mathbf{q}_{sn}^{\mathrm{T}}\right], \quad \mathbf{M}_s = \mathrm{diag}(\mathbf{M}_{s1}, \mathbf{M}_{s2}, \ldots, \mathbf{M}_{sn}), \quad \mathbf{Q}_s = \left[\mathbf{Q}_{s1}^{\mathrm{T}}, \mathbf{Q}_{s2}^{\mathrm{T}}, \ldots, \mathbf{Q}_{sn}^{\mathrm{T}}\right], \tag{2}$$

where $\mathbf{q}_{si}\ (i = 1, 2 \cdots, n)$ is the generalized co-ordinate of the ith segment. $\mathbf{M}_{si}$ is the generalized mass matrix of the ith segment

$$\mathbf{M}_{si} = \mathrm{diag}(m_{si}\mathbf{I}_3, \mathbf{J'}_{si}), \quad i = 1, 2, \cdots, n, \tag{3}$$

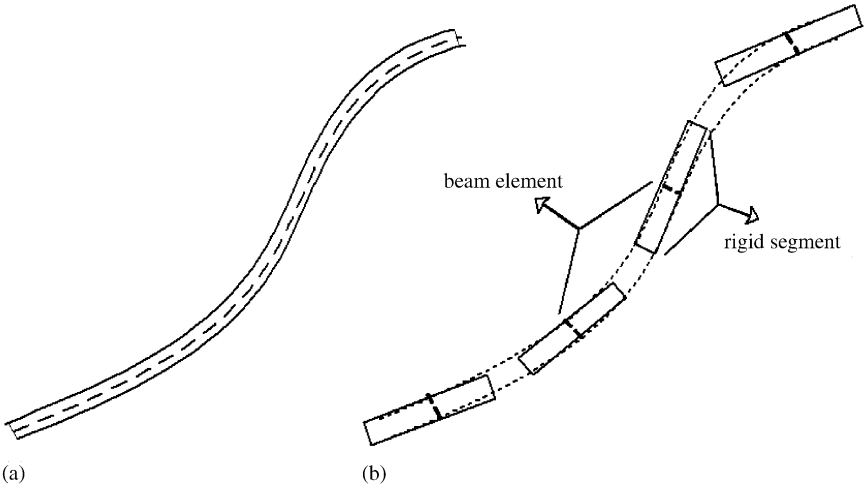

Figure 2. Finite segment model of beam like structure: (a) continuous flexible system; (b) discrete model by overlapped finite segments and elastic beam element.

where m_{si} is the mass of the segment i, $\mathbf{J'}_{si}$ the inertia tensor of the segment about its center of mass and $\mathbf{I}_3$ is the identity matrix of 3×3. $\mathbf{Q}_{si}$ $(i = 1, 2, \cdots, n)$ is generalized force of the segment including the contributions from the connecting beam elements, which are introduced in the following section.

3.1.2. *The elasticity modelling*

To account the elastic energy in the deformed flexible beam, the beam element is introduced. Consider two neighboring segments B_i and B_j in Figure 3, $B_i X_i Y_i$ and $B_j X_j Y_j$ are, respectively, the body frames with the origin at the mass center of the two segments. The element $B_i B_j$ is the elastic beam from B_i to B_j, at both ends of which, the beam has displacements consisting of segments B_i and B_j, respectively, see Figure 3. The kinetic energy of the beam is expressed in terms of the rigid segments and the elastic energy is described by the element. For the sake of simplicity, the two segments with equal length are considered.

Let O_e be the reference frame of the beam element. Its global position vector $\mathbf{r}_e$ and angles θ_e between the $\mathbf{X}_e$ and $\mathbf{X}$ axis are

$$\mathbf{r}_e = (\mathbf{r}_i + \mathbf{r}_j)/2, \quad \theta_e = (\theta_i + \theta_j)/2, \tag{4}$$

where θ_i and θ_j are, respectively, the angles $\mathbf{X}_i$ and $\mathbf{X}_j$ with respect to the $\mathbf{X}$-axis. The global position vectors and angles of the points B_i and B_j with respect to the point O_e are

$$\mathbf{a}_i = \mathbf{r}_{pi} - \mathbf{r}_e, \quad \mathbf{a}_j = \mathbf{r}_{pj} - \mathbf{r}_e, \quad \theta_i^e = \theta_i - \theta_e, \quad \theta_j^e = \theta_j - \theta_e. \tag{5}$$

In the co-ordinate system of the beam element, the above vectors are

$$\mathbf{a}_i^e = \mathbf{R}_e^{\mathrm{T}} \mathbf{a}_i = \begin{Bmatrix} \mathbf{x}_i^e \\ \mathbf{y}_i^e \end{Bmatrix}, \quad \mathbf{a}_j^e = \mathbf{R}_e^{\mathrm{T}} \mathbf{a}_j = \begin{Bmatrix} \mathbf{x}_j^e \\ \mathbf{y}_j^e \end{Bmatrix}, \tag{6}$$

where $\mathbf{R}_e$ is the transformation matrix from the beam element to global co-ordinate system.

For the beam element $B_i B_j$ shown in Figure 3, let l, E and I be, respectively, the length, elastic coefficients and area moment of inertia. Considering lateral deformation of the

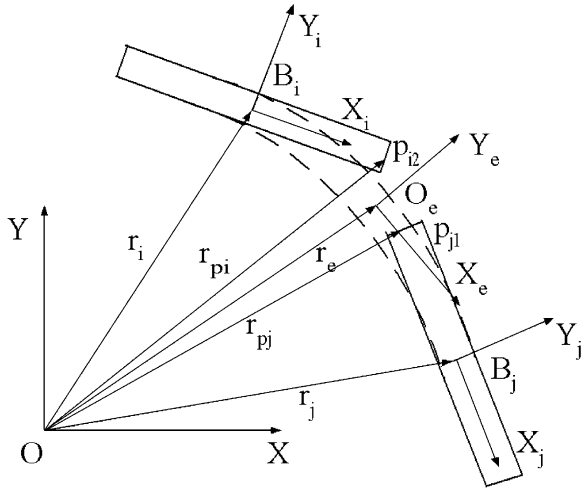

Figure 3. Two neighboring segments and the connecting beam element.

fictitious element in the co-ordinate of O_e, the following equations and bound conditions are satisfied [18]:

$$
\begin{aligned}
&EI\frac{\mathrm{d}^4 y^e}{\mathrm{d}x} = 0,\\
&y^e = y_i^e,\ \frac{\mathrm{d}y^e}{\mathrm{d}x^e} = \theta_i^e \ \text{ while } \quad x^e = -l/2,\\
&y^e = y_j^e,\ \frac{\mathrm{d}y^e}{\mathrm{d}x^e} = \theta_j^e \ \text{ while } \quad x^e = -l/2.
\end{aligned} \tag{7}
$$

As in the conventional finite element method, the force–displacement relations of the beam element can be denoted as

$$
\begin{Bmatrix} \mathbf{P}_{si}^e \\ \mathbf{P}_{sj}^e \end{Bmatrix} = \mathbf{K}^e \begin{Bmatrix} \delta_{si}^e \\ \delta_{sj}^e \end{Bmatrix}, \tag{8}
$$

where

$$
\boldsymbol{\delta}_{si}^e = \begin{Bmatrix} x_i^e \\ y_i^e \\ \theta_i^e \end{Bmatrix}, \quad \boldsymbol{\delta}_{sj}^e = \begin{Bmatrix} x_j^e \\ y_j^e \\ \theta_j^e \end{Bmatrix}, \tag{9}
$$

$$
\mathbf{P}_{si}^e = \begin{Bmatrix} F_{xi}^e \\ F_{yi}^e \\ M_i^e \end{Bmatrix}, \quad \mathbf{P}_{sj}^e = \begin{Bmatrix} F_{xj}^e \\ F_{yj}^e \\ M_j^e \end{Bmatrix}. \tag{10}
$$

When the relative deformation of the beam element is small, it can be described by the linear theories. With the cubic Hermite interpolation functions for the beam element [18] in the interval $(-1/2, 1/2)$

$$
\begin{aligned}
&\varphi_1 = \tfrac{1}{2} - \tfrac{3}{2}\xi + 2\xi^3, \quad \varphi_2 = l(\tfrac{1}{8} - \tfrac{1}{4}\xi - \tfrac{1}{2}\xi^2 + \xi^3),\\
&\varphi_3 = \tfrac{1}{2} + \tfrac{3}{2}\xi - 2\xi^3, \quad \varphi_4 = l(-\tfrac{1}{8} - \tfrac{1}{4}\xi + \tfrac{1}{2}\xi^2 + \xi^3),
\end{aligned} \tag{11}
$$

where $\xi = x/l$, the stiffness matrix of the element can be obtained as

$$\mathbf{K}^e = \begin{bmatrix} \frac{EA}{l} & 0 & 0 & -\frac{EA}{l} & 0 & 0 \\ & \frac{12EI}{l^3} & \frac{6EI}{l^2} & 0 & -\frac{12EI}{l^3} & \frac{6EI}{l^2} \\ & & \frac{4EI}{l} & 0 & -\frac{6EI}{l^2} & \frac{2EI}{l} \\ & \text{sym} & & \frac{EA}{l} & 0 & 0 \\ & & & & \frac{12EI}{l^3} & -\frac{6EI}{l^2} \\ & & & & & \frac{4EI}{l} \end{bmatrix}. \tag{12}$$

The generalized force can be transformed into the global system

$$\begin{aligned} \mathbf{Q}^e_{si} &= \mathbf{R}^e \mathbf{P}^e_{si}, \\ \mathbf{Q}^e_{sj} &= \mathbf{R}^e \mathbf{P}^e_{sj}. \end{aligned} \tag{13}$$

3.2. MATHEMATICAL MODEL FOR LOCKING IMPACTS DUE TO CLEARANCE

The locking joint with clearance is shown in Figure 4. θ_a and θ_b denote the clearance angles. When $\theta \leqslant \theta_1$, the beam enters the region of locking, and a serial of impact might take place. While the condition $\theta_a > \theta > -\theta_b$ is satisfied, the beam is in the clearance and is free from impacts. When condition $\theta \geqslant \theta_a$ or $\theta \leqslant -\theta_b$ is satisfied, the impact takes place.

The continuous contact force model with hysteresis damping in reference [16] is used for the locking joint. The original contact model is for linear contacts. In this paper, a contact model for angular contacts is presented.

The continuous contact force model in reference [15] takes the following form:

$$f = K\delta^{3/2} + D\dot{\delta}, \tag{14}$$

where δ is the local relative penetration between the surface of the two bodies. The generalized parameter K depends on the material properties and the radii (R_i, R_j) of the two spheres

$$K = \frac{4}{3\pi(h_i + h_j)} \left[\frac{R_i R_j}{R_i + R_j}\right]^{1/2}, \tag{15}$$

where the material parameters h_i and h_j are

$$h_l = \frac{1 - \mu_l^2}{\pi E_l}, \quad l = i, j. \tag{16}$$

Where μ_l and E_l are, respectively, the Poission ratio and Young's modulus associated with each body.

A hysteresis form for damping coefficient proposed by Lee and Wang [16] is

$$D = CT(\delta), \tag{17}$$

where the damping function is

$$T(\delta) = [(\delta + |\delta|)/2\delta] \exp[\{(\delta - \varepsilon) - |\delta - \varepsilon|\}(Q/\varepsilon)], \tag{18}$$

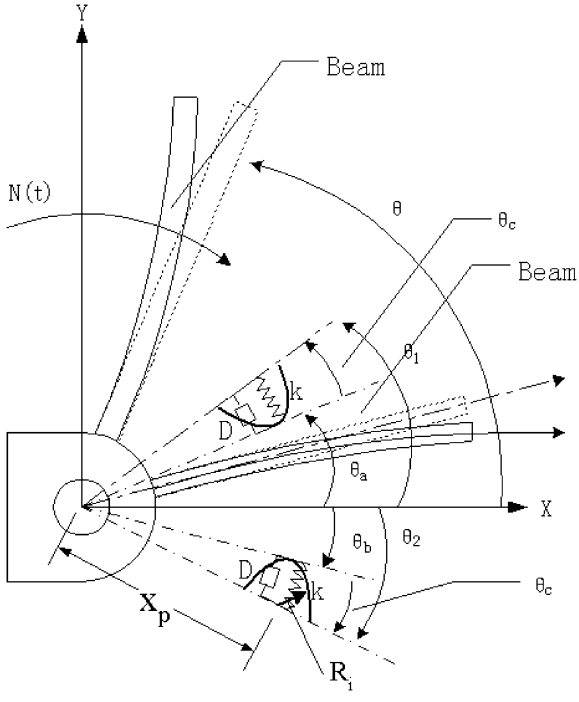

Figure 4. The sketch for locking joint with clearance.

in which ε defines a transition zone, and Q is a parameter specifying the shape of the curve within the transition zone. The damping coefficient

$$C = 2M\omega_n \sqrt{(\ln e)^2/[(\ln e)^2 + \pi^2]}, \tag{19}$$

where e is the coefficient of restitution appropriate for the initial impact velocity, and $\omega_n = \sqrt{k/M}$ is the natural frequency of the beam on the linear spring.

In the case of revolute locking joint, which has the angular form, the contact force model has to be transformed into the angular form. As shown in Figure 4, let θ_c be the angular form of the indentation δ, the following equation is obtained:

$$\theta_c = \frac{\delta}{x_p}. \tag{20}$$

The occurrence of contact between the beam and locking joint is determined by evaluating variable θ_c at any time during the numerical integration of the system equations of motion as

$$\theta_c = \begin{cases} \theta - \theta_a & \text{if } \theta \geqslant \theta_a, \\ |\theta + \theta_b| & \text{if } \theta \leqslant -\theta_b, \\ 0 & \text{if } -\theta_b < \theta < \theta_a. \end{cases} \tag{21}$$

Equation (14) has the following form:

$$f = K(x_p\theta_c)^{3/2} + CT(\theta_c)x_p\dot{\theta}_c, \tag{22}$$

where the damping function $T(\theta_c)$ is

$$T(\theta_c) = [(\theta_c + |\theta_c|)/2\theta_c] \exp[\{(\theta_c - \varepsilon_c) - |\theta_c - \varepsilon_c|\}(Q/\varepsilon_c)], \tag{23}$$

in which $\varepsilon_c = \varepsilon/x_p$.

The generalized force due to the impact between bodies i and j are

$$\mathbf{Q}_i = \begin{bmatrix} \mathbf{0} \\ \mathbf{0} \\ \mathbf{N} \end{bmatrix}, \quad \mathbf{Q}_j = -\begin{bmatrix} \mathbf{0} \\ \mathbf{0} \\ \mathbf{N} \end{bmatrix}, \tag{24}$$

where $\mathbf{N}$ is given by

$$\mathbf{N} = \begin{cases} K_t(\theta + \theta_{pre}) & \text{if } \theta > \theta_1, \\ x_p f + K_t(\theta + \theta_{pre}) & \text{if } \theta_1 \geqslant \theta \geqslant \theta_a, \\ -x_p f + K_t(\theta + \theta_{pre}) & \text{if } -\theta_2 \leqslant \theta \leqslant -\theta_b, \\ K_t(\theta + \theta_{pre}) & \text{if } \theta_b < \theta < \theta_a. \end{cases} \tag{25}$$

3.3. THE DYNAMIC EQUATIONS OF THE SYSTEM

With flexible beam modelling in section 3.1 and the impact modelling in section 3.2, the system of equations of motion can be established by the unified approach for the multi-body systems. The equations of motion of the system may be written in matrix form as [19]

$$\begin{bmatrix} \mathbf{M} & \mathbf{\Phi}_\mathbf{q}^\mathrm{T} \\ \mathbf{\Phi}_\mathbf{q} & \mathbf{0} \end{bmatrix} \begin{Bmatrix} \ddot{\mathbf{q}} \\ \boldsymbol{\lambda} \end{Bmatrix} = \begin{Bmatrix} \mathbf{Q} \\ \boldsymbol{\gamma} \end{Bmatrix}, \tag{26}$$

where $\boldsymbol{\lambda}$ is the Lagrange multiplier. The system state variable vector $\mathbf{q}$, mass matrix $\mathbf{M}$, and vector of generalized force $\mathbf{Q}$ are defined as

$$\mathbf{q} = [\mathbf{q}_1^\mathrm{T}, \mathbf{q}_2^\mathrm{T}, \ldots, \mathbf{q}_{nb}^\mathrm{T}], \quad \mathbf{M} = \mathrm{diag}(\mathbf{M}_1, \mathbf{M}_2, \ldots, \mathbf{M}_{nb}), \quad \mathbf{Q} = [\mathbf{Q}_1^\mathrm{T}, \mathbf{Q}_2^\mathrm{T}, \ldots, \mathbf{Q}_{nb}^\mathrm{T}], \tag{27}$$

in which $\mathbf{q}_i$, $\mathbf{Q}_i$ and $\mathbf{M}_i (i = 1, 2, \ldots, nb)$ are, respectively, the generalized co-ordinate, generalized force and the generalized mass matrix of the ith bodies. nb is the total rigid bodies.

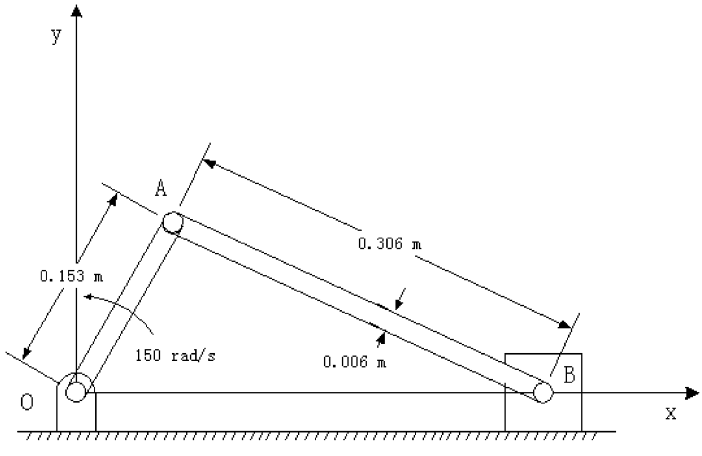

Figure 5. A slider-crank mechanism.

In equation (26), $\mathbf{\Phi_q}$ is the Jacobian matrix of the combined constraint equations

$$\mathbf{\Phi}(\mathbf{q}, t) = \mathbf{0} \tag{28}$$

and

$$\boldsymbol{\gamma} = -(\mathbf{\Phi_q}\dot{\mathbf{q}})_{\mathbf{q}}\dot{\mathbf{q}} - 2\mathbf{\Phi}_{\mathbf{q}t}\dot{\mathbf{q}} - \mathbf{\Phi}_{tt}. \tag{29}$$

The effect of the elastic force and that of the impact force can be accounted by inserting the generalized forces of equations (13) and (24) into the right-hand side of equation (28) in the integration.

4. NUMERICAL IMPLEMENTATION

The fourth order variable step Runge–Kutta algorithm and the generalized co-ordinate partitioning approach [19] are used to solve the differential–algebraic equations (26). The algorithms are implemented with the object-oriented C++ language.

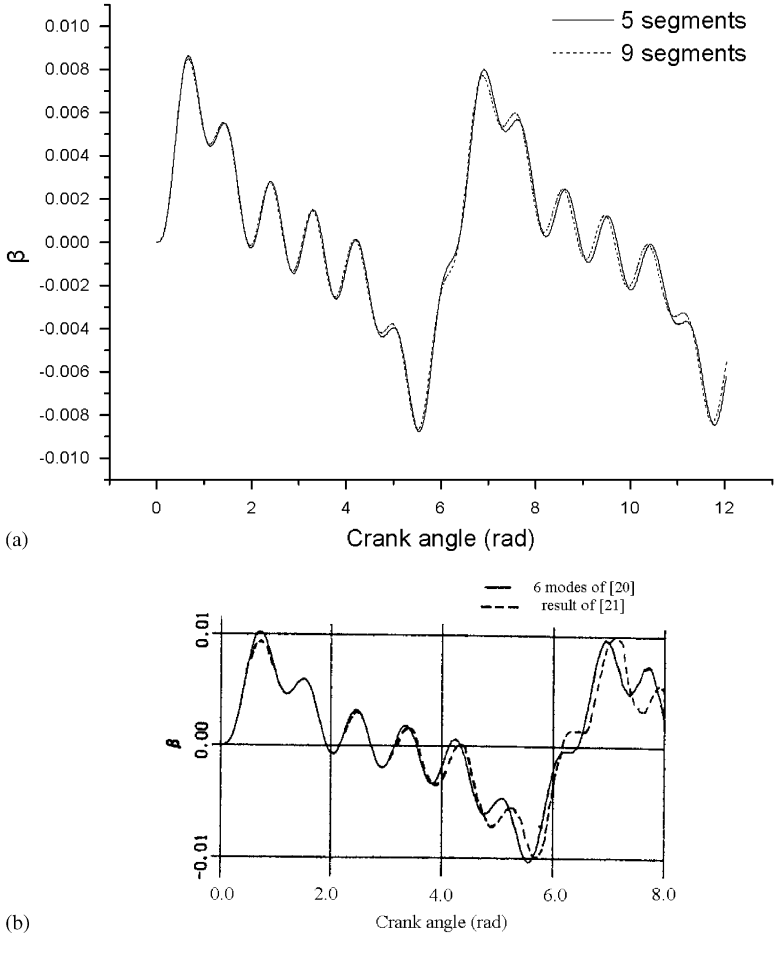

Figure 6. Transverse deformation of the connecting rod: (a) results of this paper; (b) result of references [20, 21].

Generally, the axial dynamics of the flexible beam is of very high frequencies, and it poses stiff problem with the rigid-body motions. But in many cases, the axial deformation of a beam is negligible. In the numerical solution, a constraint that eliminates the axial deformation of the beam is presented to decrease the stiffness of the equations.

4.1. A CONSTRAINT FOR DECREASING THE STIFFNESS OF THE EQUATIONS OF MOTION

The longitudinal constraint for the element B_iB_j is defined as

$$\mathbf{\Phi} = (\mathbf{r}_j - \mathbf{r}_i) \cdot \mathbf{e}_{x_i} - l = 0, \tag{30}$$

where $\mathbf{e}_{x_i}$ is the unit vector along B_iX_i. The corresponding Jacobian $\mathbf{\Phi}_\mathbf{q}$ is

$$\mathbf{\Phi}_\mathbf{q} = [-\cos\theta_i - \sin\theta_i - (x_j - x_i)\sin\theta_i + (y_j - y_i)\cos\theta_i - \cos\theta_i \quad -\sin\theta_i \quad 0], \tag{31}$$

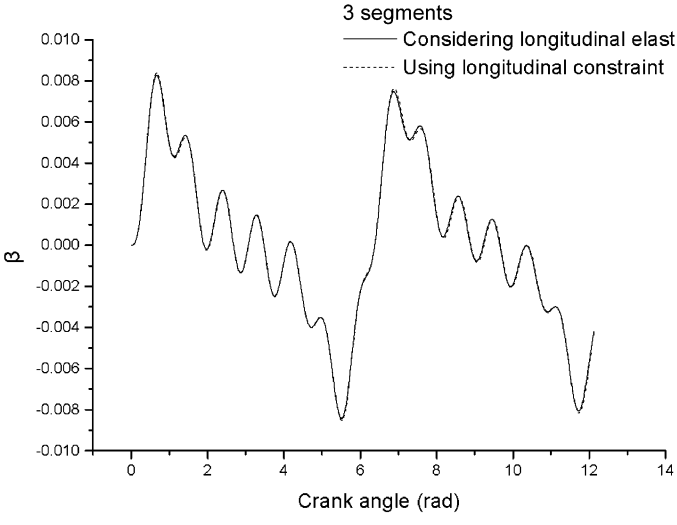

Figure 7. The comparison of β with and without longitudinal constraint.

TABLE 1

Physical parameters of the system

Body no.	Mass (kg)	Inertia (kg m^2)	Length (m)
Central body	36	0·38	0·32
Beam 1	0·424	0·0226	0·8
Beam 2	0·424	0·0226	0·8
Beam 3	0·424	0·0226	0·8
Beam 4	0·382	0·0204	0·8
Joint 1	0·306	0·00025	0·04
Joint 2	0·306	0·00025	0·04
Joint 3	0·306	0·00025	0·04
Joint 4	0·306	0·00025	0·04

where $\mathbf{q}$ is the generalized co-ordinate. The velocity equation and the acceleration equation of the constraint are, respectively,

$$\mathbf{\Phi}_{\mathbf{q}}\dot{\mathbf{q}} \equiv \boldsymbol{\nu} = \mathbf{0}, \tag{32}$$

$$\mathbf{\Phi}_{\mathbf{q}}\ddot{\mathbf{q}} \equiv \boldsymbol{\gamma} = 2(\dot{x}_j - \dot{x}_i)\dot{\theta}_i \sin\theta_i - 2(\dot{y}_j - \dot{y}_i)\dot{\theta}_i \cos\theta_i + \left[(x_j - x_i)\cos\theta_i + (y_j - y_i)\sin\theta_i\right]\dot{\theta}_i^2. \tag{33}$$

4.2. NUMERICAL EXAMPLE

The slider-crank mechanism [20] shown in Figure 5 is used to assess the validity of the presented modelling method. The mechanism consists of the rigid crank OA of length L_a, a connecting rod AB of uniform circular cross-section and length L_b, and a sliding block

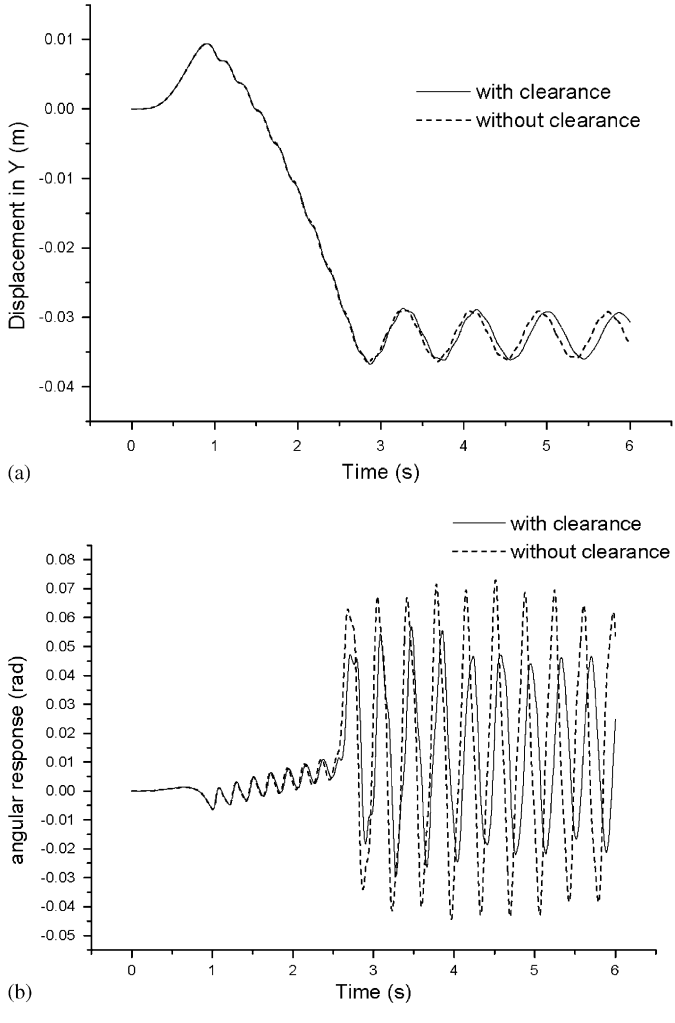

Figure 8. Response of central rigid-body: (a) response of the displacement in the Y direction; (b) angular response around its center of mass.

located at B. The elastic connecting rod is assumed initially straight and simply supported at the ends of pins. Transverse and axial deformations of the connecting rod in the plate are allowed. The connecting rod is a steel bar. The slider-crack maintains a constant angular velocity of 150 rad/s. Other parameters for this example are: $m_{OA} = m_B = 0{\cdot}038$ kg, $m_{AB} = 0{\cdot}076$ kg, $J_{OA} = 7{\cdot}4 \times 10^{-5}$ kg m^2, $J_{AB} = 5.9 \times 10^{-4}$ kg m^2 and $J_B = 1{\cdot}8 \times 10^{-6}$ kg m^2. J_{OA}, J_{AB} and J_B are, respectively, the moment of inertia about the center of mass of bar OA, AB and sliding block B.

The transverse deflection of the connecting rod at its midpoint is represented by the dimensionless parameter β, i.e., the ratio of the actual deflection to the length of the connecting rod. Figure 6(a) depicts the results on the transverse deformation of the rod by five segments and nine segments models respectively. For comparison, 6-mode solutions from reference [20] and the results of reference [21] are also presented in Figure 6(b).

Figure 7 compares deflection considering longitudinal elasticity and using longitudinal constraint (3-segments). The difference is negligible. The CPU time by using longitudinal constraint is only 20% of that for considering longitudinal elasticity.

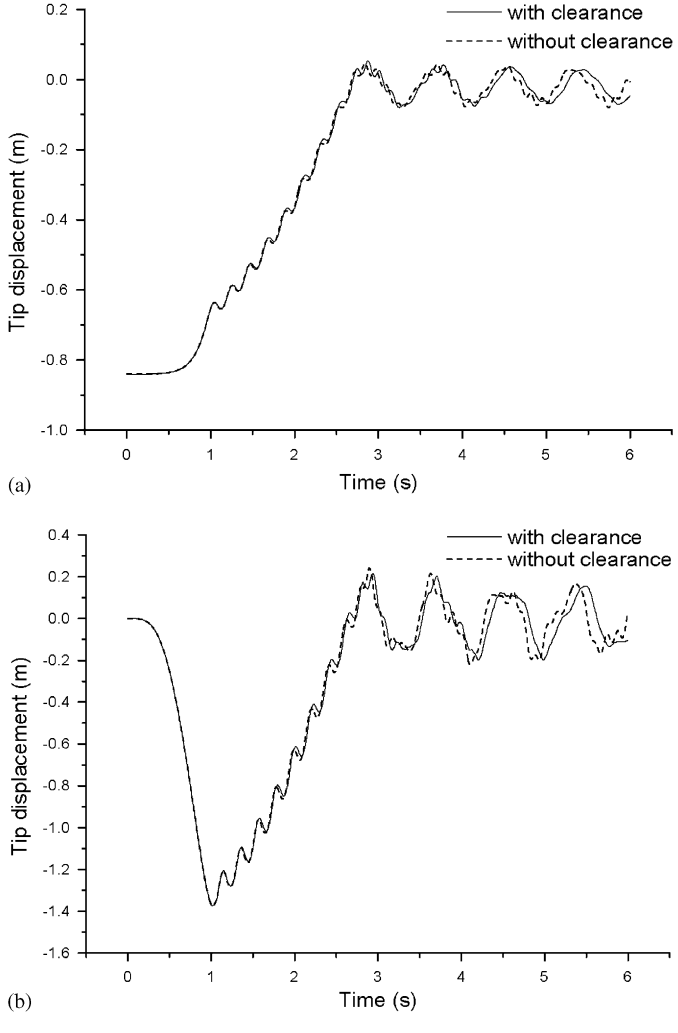

Figure 9. Response of the tip displacement: (a) response of beam 1; (b) response of beam 2.

5. SIMULATION OF THE DEPLOYMENT SYSTEM

In this section, the simulation results on the flexible deployment system described in section 2 are presented. The simulation results with and without clearance are presented. The physical parameters of the system are presented in Table 1. These parameters are the actual values from the physical model. The area moments of inertia of beams 1–3 are $2{\cdot}71 \times 10^{-10}\ \mathrm{m}^4$, and that of beam 4 is $2{\cdot}52 \times 10^{-10}\ \mathrm{m}^4$. In the simulation, each beam is divided into four segments and each joint is divided into two rigid bodies connected by locking joint. The elastic parameter E_i for the joints (see section 3.2) is $2{\cdot}01 \times 10^{11}\ \mathrm{N/m}^2$

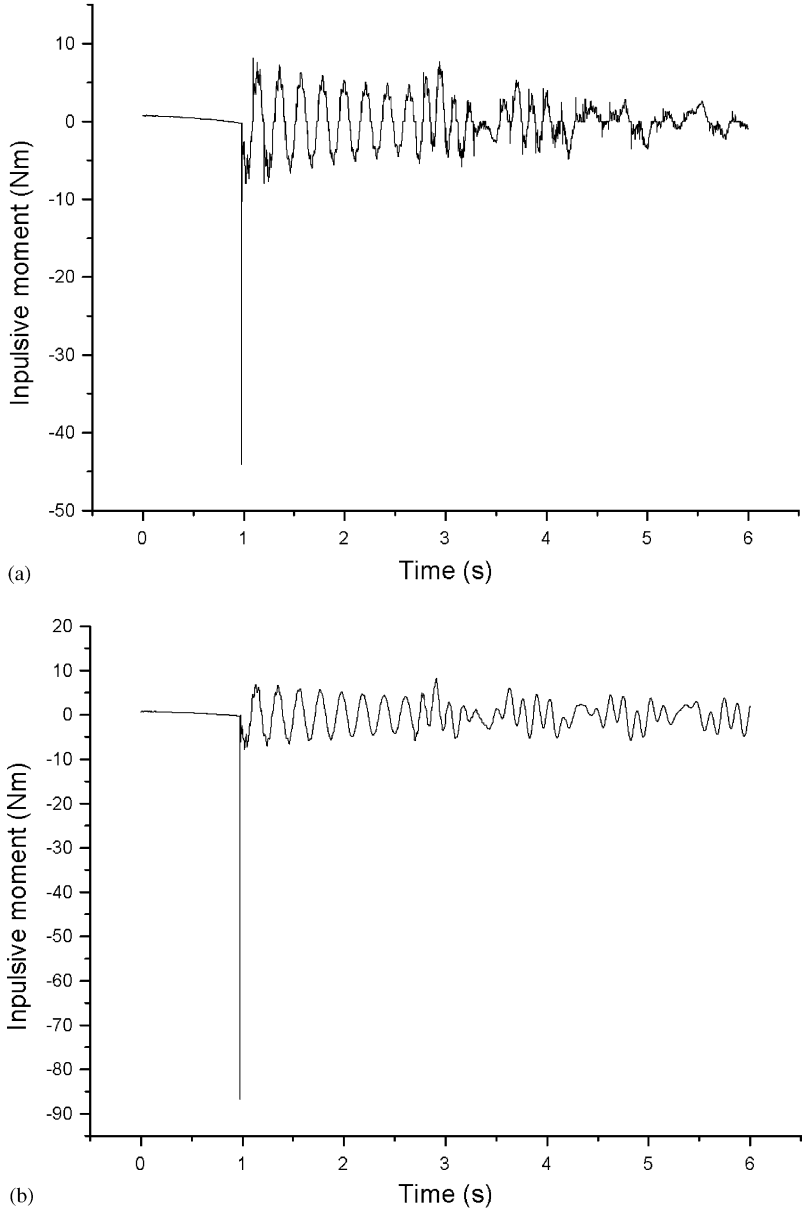

Figure 10. The impulsive moment at joint 2: (a) with clearance; (b) without clearance.

and E_j for the beams is $6{\cdot}895 \times 10^{10}\,\mathrm{N/m^2}$. The measured clearance of these joints is $\theta_a = \theta_b = 0{\cdot}0052$ rad. Other parameters are as follows $\mu_i = \mu_j = 0.3$, $Q = 3{\cdot}0$, $\varepsilon = 0{\cdot}5 \times 10^{-5}$ m, $R_i = 0{\cdot}005$ m, $R_j \gg R_i$, $e = 0{\cdot}85$ and $k = 3{\cdot}2 \times 10^9\,\mathrm{N/m}$. The angular stiffness of the springs in the locking joints is $0{\cdot}218\,\mathrm{N\,m/rad}$, and the pre-compressed angle $\theta_{pre} = 1{\cdot}57$ rad.

Figure 8(a) presents the response of the displacement of the central rigid-body in the Y direction. Figure 8(b) presents the rotation of the central rigid-body around its center of mass. As the beams on the two sides of the central rigid-body are not symmetric, the central rigid-body oscillates during the deployment. As can be seen from the responses, the

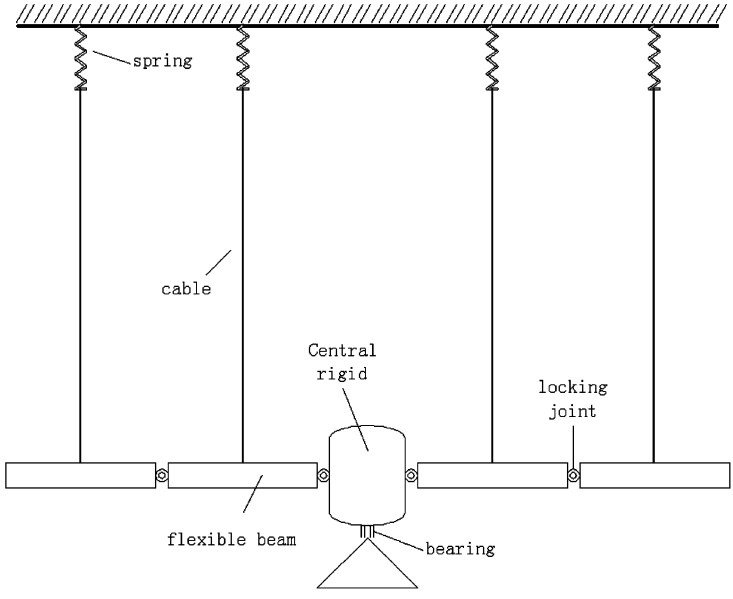

Figure 11. The sketch of the experimental set-up.

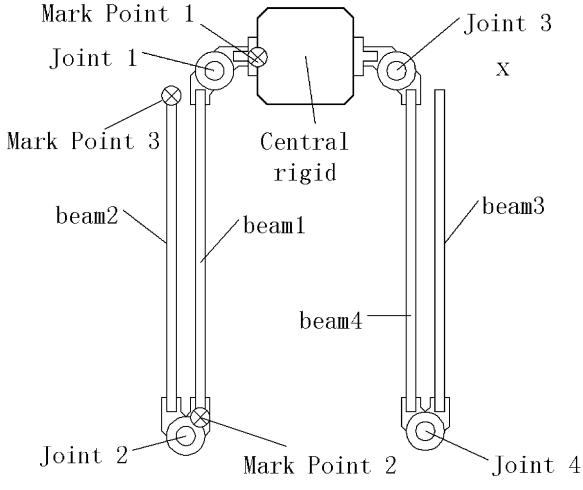

Figure 12. The initial configuration and mark points.

clearance in the joints decreases the vibration frequency of the system and the amplitude of the central rigid-body. This indicates that presence of the clearance has softening effects on the system stiffness. The effect on the amplitude of the central rigid-body might attribute to the reduction in the interaction between the beams and the rigid-body by clearances.

Figure 9(a) and (b) presents the responses of the tip displacement of beams 1 and 2 respectively. It is also indicated that the clearance decreases the vibration frequency of the system slightly.

Figure 10(a) and (b) presents impulsive moment of joint 2 by using the contract force model with hysteresis damping. The results show that the peak value of the impulsive moment in the joint locking is decreased due to clearance. However, multi-impacts are observed in the post-locking responses when the clearances are presented, hence, arising small sharp peaks in the contacting moments, see Figure 10(a).

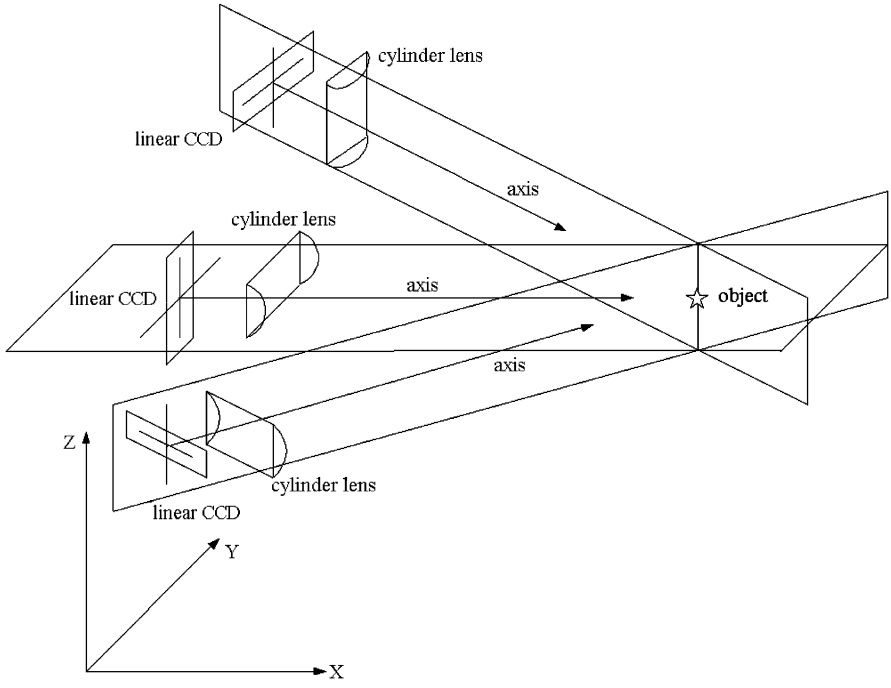

Figure 13. The positioning system of linear CCD cameras.

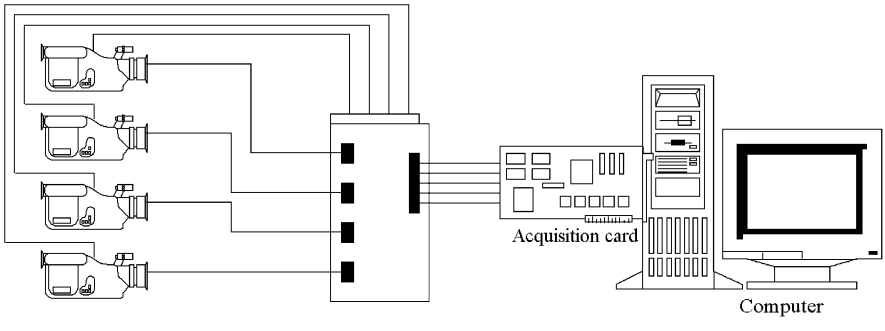

Figure 14. Instrumentation block diagram.

6. EXPERIMENT SET-UP OF THE DEPLOYMENT SYSTEM

6.1. EXPERIMENTAL SET-UP

The schematic diagram of the experimental set-up of the deployed system is shown in Figure 11. The beams are suspended with light strings to alleviate the effect of gravity. The length of the strings is 7 m. For the response vibration induced by the deployment and locking impact, the influence of the suspension can be ignored.

The parameters of the four flexible aluminum beams, locking joints and central rigid-body are shown in Table 1. The stiffness of torsion spring in the locking joint is 0·218 N m/rad. The clearance of the joint after locking is 0·0104 rad. Three LEDs are used to mark measured points on the central rigid-body, joint 2 and the tip of beam 2, respectively, see Figure 12.

6.2. NON-CONTACT THREE-DIMENSIONAL REAL-TIME POSITIONING SYSTEM

An optical measurement system, non-contact three-dimensional real-time positioning system of multiple light-spots by three linear CCD cameras, is used for measuring the response of deployment as shown in Figure 13. The imaging system consists of cylinder lens. Three CCD cameras are sufficient to resolve the spatial co-ordinates of a measured point. The fourth CCD is used as a means for compensating noises, see Figure 14.

The linear CCD used in the system is TCD1206 with 2160 pixels. The measurement system is calibrated with a high precision total station. The accuracy of positioning system is 5 mm in a $2000 \times 2000 \times 2000\,\text{mm}^3$ space. This corresponds to a spatial resolution of about 0.25% overall accuracy.

7. EXPERIMENTAL RESULTS AND CORRELATION

The simulated results are compared with the available experimental results at the three points on the system. The angular response of the central rigid-body is shown in Figure 15.

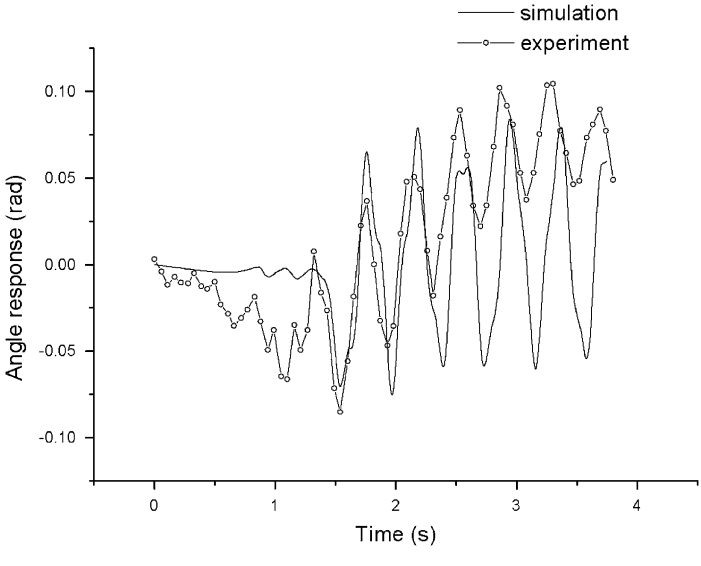

Figure 15. Response of central rigid-body.

The displacement of mark points 2 and 3 are compared in Figure 16. The mathematical model presented in this paper captures the overall feature of the responses.

In the simulation, every flexible beam is divided into eight segments and the effects of the suspension string are considered by incorporating the pendulum restoring forces of the string.

The frequency response spectrum of the simulation and experimental results by FFT are also presented in Figure 17. As observed, the frequency spectra from the results of eight segments model coincide very well with that from experiments.

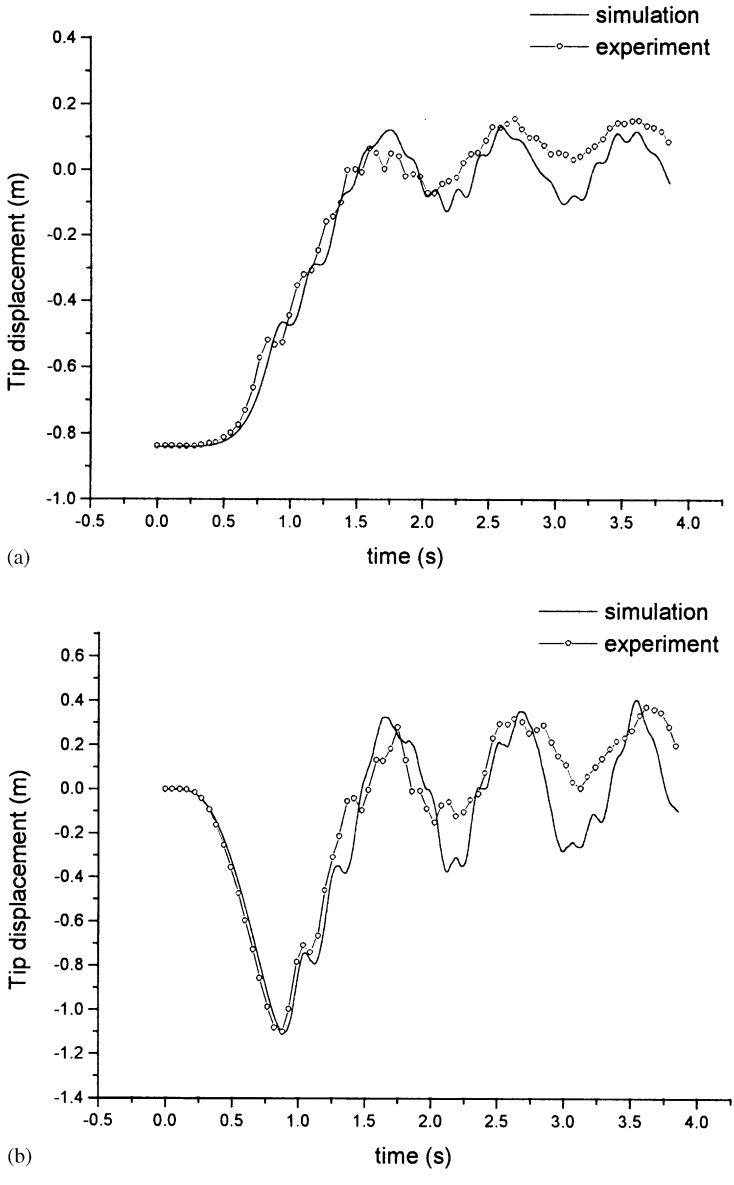

Figure 16. Response of displacement of the mark points 2 and 3: (a) point 2; (b) point 3.

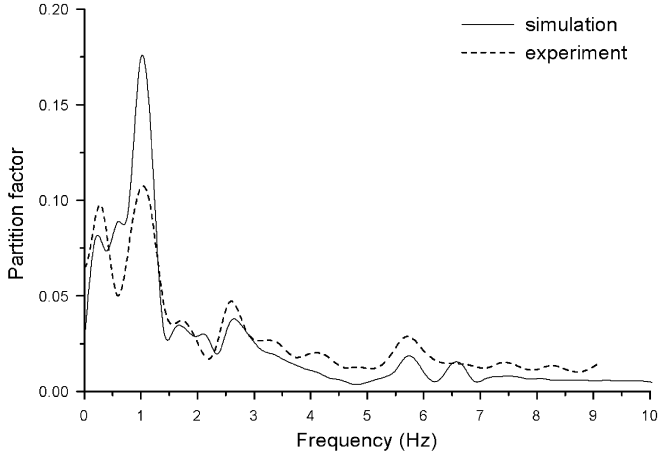

Figure 17. Frequency spectrum.

8. CONCLUSIONS

In this paper, a hybrid finite segment/finite element approach is proposed for modelling the large motion flexible beam in a deployment system. The method uses the finite segments to describe the inertia of the large motion beam and enables a small deformation theory for describing the elasticity of the beam in the relative co-ordinate systems. Application of this method to a verification example yields comparable results with the available literatures and the convergence of the method is satisfactory. Simulations also show that the longitudinal constraint accelerates the numerical solution.

Together with the contact force model of the impact, this method is used to analyze the deployment of a system with internal impact in the joints. The simulated results show that the clearance decreases both the vibration frequency of the system and the peak value of the impulsive moment of locking, as well as the vibration amplitude of the central rigid-body. Also observed are the multi-impacts induced by the clearances in the joints.

The simulation with the presented methods demonstrates robustness in the experimented deployment system. The correlation between the simulation and the experiment shows that the mathematical model developed in this paper can give reasonable results for the studied deployment system.

ACKNOWLEDGMENTS

This work was done under the support of Natural Science Foundation of China (Grant No. 19802010 and 10172049).

REFERENCES

1. A. A. Shabana 1989 *Dynamics of Multibody System*. New York: John Wiley & Sons, Inc.
2. Y. A. Khulief 1992 *Computer Methods in Applied Mechanics and Engineering* **97**, 23–32. On the finite element dynamic analysis of flexible mechanisms.
3. W. Pan and E. J. Haug 1999 *Computer Methods in Applied Mechanics and Engineering* **173**, 189–200. Flexible multibody dynamic simulation using optimal lumped inertia matrices.

4. Y. KHULIEF 2000 *Multibody System Dynamics* **4**, 383–406. Spatial formulation of elastic multibody systems with impulsive constraints.
5. E. M. BAKR and A. A. SHABANA 1986 *Computers and Structures* **23**, 739–751. Geomerically non-linear analysis of multibody systems.
6. R. L. HUSTON 1990 *Multibody Dynamics*. Boston: Butterworth-Heinemann.
7. J. D. CONNELLY and R. L. HUSTON 1994 *Computers and Structures* **50**, 255–258. The dynamics of flexible multibody systems—a finite segment approach. 1: theoretical aspects.
8. J. D. CONNELLY and R. L. HUSTON 1994 *Computers and Structures* **50**, 259–262. The dynamics of flexible multibody systems-a finite segment approach. 2. example problems.
9. E. ZAKHARIEV 2000 *Mechanics of Structures and Machines* **28**, 105–136. Non-linear dynamics of rigid and flexible multibody systems.
10. Y. A. KHULIEF and A. A. SHABANA 1986 *Journal of Sound and Vibration* **104**, 187–207. Impact responses of flexible multibody systems with consistent and lumped masses.
11. J. RISMANTAB-SANY and A. A. SHABABA 1990 *American Society of Mechanical Engineers Journal of Vibration and Acoutics* **112**, 119–125. On the use of the momentum balance in the impact analysis of constrained elastic systems.
12. Y. KHULIEF and A. A. SHABANA 1986 *Journal of Mechanics Transmission and Automatic Design* **108**, 38–45. Dynamic analysis of constrained system of rigid and flexible bodies with intermittent motion.
13. B. P. NAGARAJ, B. S. NAGARAJ and A. GHOSAL 1997 *Journal of Sound and Vibration* **207**, 567–589. Dynamics of a two-link flexible system undergoing locking: mathematical modelling and comparison with experiments.
14. S. DUBOWSKY and T. N. GARDNER 1975 *Journal of Engineering for Industry* **97B**, 652–661. Dynamic interactions of link elasticity and clearance connections in planar mechanical systems.
15. K. H. HUNT and F. R. E. CROSSLEY 1975 *Journal of Applied Mechanics* **42E**, 440–456. Coefficient of restitution interpreted as damping in vibroimpact.
16. T. W. LEE and A. C. WANG 1983 *Journal of Mechanisms, Transmissions, and Automation in Design* **105**, 534–540. On the dynamics of intermittent-motion mechanism. Part 1: dynamics model and response.
17. A. S. YIGIT, A. G. ULSOY and R. A. SCOTT 1990 *Journal of Sound and Vibration* **142**, 515–525. Spring-dashpot models for the dynamics of a radially rotating beam with impact.
18. H. I. LAURSEN 1988 *Structural Analysis*. New York: McGraw-Hill Book Company; third edition.
19. E. J. HAUG 1990 *Computer-Aided Kinematics and Dynamics of Mechanical Systems Volume* 1: *Basic Methods*. Boston: Allyn and Bacon.
20. A. A. SHABANA and R. WEHAGE 1983 *Journal of Mechanics Transmission and Automatic Design* **105**, 371–378. A variable degree of freedom component mode analysis of inertia variant flexible mechanical systems.
21. J. O. SONG and E. J. HAUG 1980 *Computer Methods in Applied Mechanics and Engineering* **24**, 350–381. Dynamic analysis of planar flexible mechanisms.